Transp Porous Med (2014) 105:559–570
DOI 10.1007/s11242-014-0384-6

Radial Flow of Non-Newtonian Power-Law Fluid in a Rough-Walled Fracture: Effect of Fluid Rheology

Alexandre Lavrov

Received: 13 August 2013 / Accepted: 22 August 2014 / Published online: 2 September 2014

Abstract Fluid flow in a single rough-walled rock fracture has been extensively studied over the last three decades. All but few of these studies, however, have been done with Newtonian fluids and unidirectional flow in rectangular fractures. Notwithstanding the importance of such setups for theoretical understanding of fundamental issues in fracture flow, practical applications in drilling and petroleum engineering often involve radial flow of a non-Newtonian fluid. An example is a borehole intersecting a natural fracture during drilling in a fractured rock. In this study, steady-state incompressible radial flow from a circular well into a self-affine rough-walled fracture was simulated numerically using the lubrication theory approximation. The fluid rheology was power law. The flow behavior index was equal to 0.6, 0.8, 1.0 (Newtonian), 1.2, or 1.4. Asperities diverted the flow from an axisymmetric radial pattern that would be observed in a smooth-walled fracture. The extent of the deviation from radial flow was found to increase as the fluid became more shear-thickening. To reveal finer details of the flow, a tracer was introduced at the borehole wall and was transported by the flow. The front of the tracer propagating into the fracture was found to become slightly smoother with a more shear-thickening fluid. In the vicinity of contacts between fracture faces a more shear-thickening fluid could deliver the tracer closer to the contact spots.

Keywords Non-Newtonian · Fluid · Flow · Rock · Fracture

1 Introduction

Single-phase or multiphase Newtonian fluid flow in a single rough-walled fracture has been the subject of experimental and numerical studies in the last 30 years (e.g., Neuzil and Tracy 1981; Brown 1987; Nicholl and Glass 2001; Glass et al. 2001; Schmittbuhl et al. 2008; Koyama et al. 2009; Vilarrasa et al. 2011; Yang et al. 2013). These studies typically involved a rectangular fracture and unidirectional flow, i.e., a pressure gradient was applied

A. Lavrov (✉)
Formation Physics Department, SINTEF Petroleum Research, Trondheim, Norway
e-mail: alexandre.lavrov@sintef.no

between two opposite sides of the rectangle with zero flux boundary conditions applied on two other opposite sides. This geometry is convenient in experiments and, probably even so, in numerical studies where it enables an easy application of boundary conditions in either a finite difference or a finite-volume numerical scheme. In many practical situations, however, e.g., when a natural fracture is intersected by a borehole during drilling, the flow into the fracture is radial rather than unidirectional. In addition, non-Newtonian fluids are commonly employed in oil and gas industry. Examples are drilling fluids and fluids used in well stimulation (e.g., fracking fluids). Therefore, notwithstanding considerable importance of the above-mentioned studies for our understanding of fundamental aspects of fracture flow, practical applications require that non-Newtonian fluids and radial geometry eventually be considered. Understanding radial flow of non-Newtonian fluids in rough-walled fractures is important, in particular, for the design of drilling fluids and well stimulation treatments. It should be mentioned that non-Newtonian, shear-thinning fluid rheology is crucial for the very operation of drilling fluids. It prevents drilling cuttings from sedimentation when circulation is stopped. It also prevents the drilling fluid from propagating indefinitely in natural fractures met by the borehole during overbalanced drilling, i.e., with the borehole pressure being higher than the pore pressure in the formation.

So far, only few experimental (Auradou et al. 2008, 2010) and numerical (Federico 1997; Lavrov 2013a, b) studies of non-Newtonian power-law fluid flow in rough-walled fractures have been accomplished. A rectangular setup described above in the context of Newtonian fluids was used in all these studies. The fluid rheology (shear-thinning versus shear-thickening) was found to affect both the effective hydraulic aperture and the details of the flow pattern. In particular, the flow was found to become more unidirectional as the fluid became more shear-thinning.

With regard to radial geometry, a numerical study of Newtonian fluid flow into a rough-walled fracture from a well of rectangular cross-section was performed by Koyama et al. (2006). Radially symmetric flow of a non-Newtonian fluid in a smooth-walled fracture was analyzed numerically by Majidi et al. (2010). Radial flow of a Newtonian fluid into a rough-walled fracture was studied experimentally by Yeo et al. (1998), Esaki et al. (1999), Mitani et al. (2002), and Cheon et al. (2002) and numerically by Koyama et al. (2004) and Vilarrasa (2005).

The objectives of the work presented herein were:

to set up, probably for the first time, a numerical model of steady-state *radial* flow of a *non-Newtonian power-law fluid* from a circular well into a rough-walled fracture;

to perform an initial investigation of the effect the fluid rheology might have on the radial flow pattern in the fracture.

2 Numerical Model, Simulation Setup, and Data Processing

The fracture generation procedure was similar to those used earlier by e.g., Brown (1987) and Lavrov (2013a, b). Two rectangular self-affine surfaces with 65×65 nodes were generated numerically using recursive subdivision technique with the Hurst exponent equal to 0.7 (Fournier et al. 1982). The surfaces were then subtracted from each other. The aperture was set equal to a negligible value (10^{-9} m) where such subtraction produced negative or zero values, i.e., at contact overlaps. Similar treatment of contacts can be found in earlier numerical studies of flow in fractures, e.g., Brown (1987). Setting the aperture at contacts to a small but non-zero value makes it possible to include these spots in the computation domain instead of applying boundary conditions along the boundaries of contact areas.

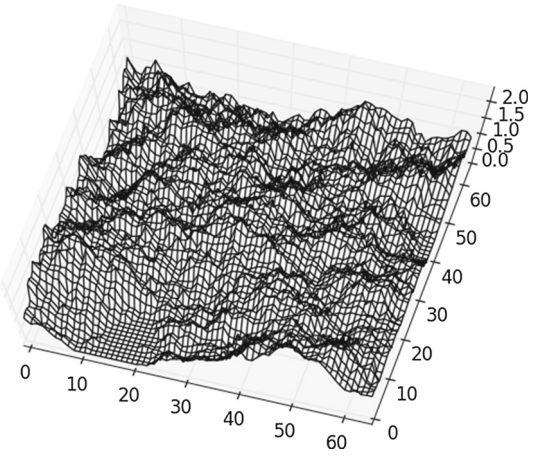

Fig. 1 Distribution of fracture aperture before circular boundaries are introduced. In-plane fracture dimensions are in cm. Aperture is in mm

The grid spacing was equal to $\Delta x = \Delta y = 0.01$ m, the fracture in-plane dimensions thus being 0.64 m $\times$ 0.64 m. This might appear a relatively small fracture since many natural fractures extend for dozens or hundreds of meters. However, plugging of the fracture by mud additives occurs in the immediate vicinity of the well (Guo et al. 2014). Therefore, it is the near-well area that is usually in focus in drilling fluids engineering. Moreover, some techniques used to control or prevent mud losses in the industry, e.g., wellbore strengthening, aim at creating a man-made short fracture in a controlled way so as to plug it and prevent more severe uncontrolled fracturing during subsequent drilling. The fracture size in wellbore strengthening is believed to be quite small, on the order of 6 inches (Aston and McLean 2004). Finally, this is a demonstration study and does not aim at a large scale simulation of non-Newtonian fluid flow in fractures. Therefore, the choice of the domain 0.64 m $\times$ 0.64 m appears to be reasonable.

The fracture aperture distribution is shown in Fig. 1. An area of contact overlap appears near the left bottom corner of the fracture. The in-plane coordinates x and y have the origin in the left bottom corner of the fracture plane. The average aperture of the fracture was equal to 0.898 mm. The standard deviation of the aperture was rms = 0.427 mm, the ratio rms$/\Delta x$ thus being equal to 0.0427. The roughness of the fracture aperture profile was thus small enough for the lubrication theory approximation to be valid [for a detailed discussion of the lubrication theory validity criteria see e.g., Zimmerman et al. (1991)]. Note that these criteria were developed by Zimmerman et al. (1991) for *Newtonian* fluids. Therefore, as pointed out by Lavrov (2013b), their direct application for non-Newtonian fluids is still an open question.

A circular well having a diameter of 0.2 m and centered at $x = y = 0.32$ m was placed in the model by eliminating all grid points that happened to be within the circle. In a similar way, a circular external boundary was introduced by eliminating all nodes that happened to be outside the circle of 0.6 m in diameter centered at $x = y = 0.32$ m. Pressure boundary conditions were applied at both the well boundary and the external boundary. The (constant) borehole pressure was equal to 2 Pa; the pressure applied at the external boundary was equal to 1 Pa, the flow thus being outwards from the well. The flow problem was steady state, incompressible flow. With the lubrication theory approximation providing the local solution to the momentum conservation equation, the mass conservation equation in Cartesian coordinates read (Lavrov 2013a):

Table 1 Shear stress (τ_{xy}) versus shear rate ($\dot{\gamma}_{xy}$) dependences in a simple shear flow in xy-plane for five fluids used in the simulations

Flow behavior index, n	Shear stress versus shear rate
0.6	$\tau_{xy} = C\left(\dot{\gamma}_{xy}\right)^{0.6}$
0.8	$\tau_{xy} = C\left(\dot{\gamma}_{xy}\right)^{0.8}$
1.0 (Newtonian fluid)	$\tau_{xy} = C\dot{\gamma}_{xy}$, C has the meaning of dynamic viscosity in this case
1.2	$\tau_{xy} = C\left(\dot{\gamma}_{xy}\right)^{1.2}$
1.4	$\tau_{xy} = C\left(\dot{\gamma}_{xy}\right)^{1.4}$

$$-\frac{\partial}{\partial x}\left(\frac{n}{2n+1}\frac{w^{(2n+1)/n}}{C^{1/n}2^{(n+1)/n}\left((\partial p/\partial x)^2+(\partial p/\partial y)^2\right)^{\frac{n-1}{2n}}}\frac{\partial p}{\partial x}\right)$$
$$-\frac{\partial}{\partial y}\left(\frac{n}{2n+1}\frac{w^{(2n+1)/n}}{C^{1/n}2^{(n+1)/n}\left((\partial p/\partial x)^2+(\partial p/\partial y)^2\right)^{\frac{n-1}{2n}}}\frac{\partial p}{\partial y}\right)=0, \tag{1}$$

where x and y are in-plane coordinates; w is the (out-of-plane) fracture aperture; p is the fluid pressure; C and n are the fluid consistency index and the (dimensionless) fluid flow behavior index of the power-law fluid, respectively. These two parameters define the shear stress, τ_{ij}, as a function of the shear rate, $\dot{\gamma}_{ij}$, as follows:

$$\tau_{ij} = C\dot{\gamma}^{n-1}\dot{\gamma}_{ij}, \tag{2}$$

where

$$\dot{\gamma} = \sqrt{2\mathbf{D}:\mathbf{D}} \tag{3}$$

and $\mathbf{D}$ is the strain rate tensor. At $n < 1$, the fluid is shear-thinning; at $n > 1$, the fluid is shear-thickening. If $n = 1.0$, the fluid is Newtonian, and the consistency index, C, is the dynamic viscosity of the fluid in this case.

Equation (1) with constant pressure boundary conditions was solved numerically on a regular Cartesian grid using a finite-volume fixed-point solver. A second-order discretization of Eq. (1) was used. The iterations were performed until convergence in pressure was reached (relative variation in pressure below a pre-defined tolerance), but only if the global mass conservation was satisfied (equal flux through contours surrounding the borehole). Further details of the numerical scheme can be found in (Lavrov 2013a). For a detailed discussion of numerical schemes available for non-Newtonian fluid flow in porous media, the reader is referred to Balhoff et al. (2012).

Five simulations were performed, with n equal to 0.6, 0.8, 1.0 (Newtonian), 1.2, or 1.4. Shear stress versus shear rate dependences of these three fluids in a simple shear flow are summarized in Table 1. This range covers the values of n typical of applications in e.g., hydraulic fracturing. Distributions of the fluid pressure and velocity were reported at the end of the flow field computation in each simulation. During data processing, for each grid node, the angle, α, between the fluid velocity in that node and the radius-vector from the well center to that node was evaluated. The velocity field was compared to a perfectly radial velocity field by evaluating the following three parameters for each simulation: (i) average value of α in the flow computation domain, $\langle\alpha\rangle$; (ii) average value of absolute α in the flow computation domain, $\langle|\alpha|\rangle$; (iii) standard deviation of α, $\sigma = \sqrt{\sum_{i=1}^{N}(\alpha_i - \langle\alpha\rangle)^2/(N-1)}$, in the flow

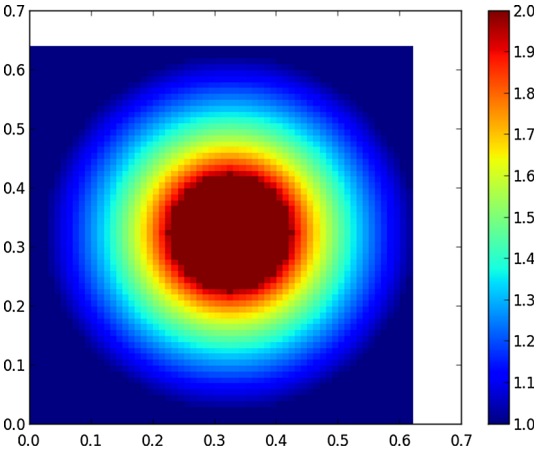

Fig. 2 In-plane distribution of the fluid pressure in a smooth-walled fracture of constant aperture. Color bar fluid pressure in Pa. *Axes* indicate coordinates (m) with the origin in the *bottom left corner*

computation domain. In the last expression, $N = 2500$ is the number of grid nodes in the flow computation domain, and the summation is over grid nodes in that domain. The flow computation domain was defined as the set of grid nodes located between the well boundary and the circular external boundary. In a perfectly radial flow, i.e., for a fracture with smooth parallel walls, one would obtain $\langle \alpha \rangle = \langle |\alpha| \rangle = \sigma = 0$.

In order to better visualize the flow pattern, the steady-state simulations were supplemented with tracer transport simulations. Once the steady flow was established, a tracer with a (normalized) concentration of $c = 1.0$ was introduced at the borehole boundary. Propagation of the tracer concentration front was computed by numerically solving the incompressible advection equation:

$$\frac{\partial c}{\partial t} + \mathbf{v} \cdot \nabla c = 0, \tag{4}$$

where $\mathbf{v}$ is the fluid velocity. Here, and in the remainder of the paper, the fluid velocity refers to the local fluid velocity averaged along the fracture aperture. It is thus essentially the flow rate divided by the aperture. Equation (4) was solved using a semi-Lagrangian method with cubic Lagrangian interpolation (Staniforth and Côté 1991; Lavrov 2009). The external circular boundary was a sink for c. Next section presents the main findings obtained in the simulations.

3 Results and Discussion

The accuracy of representing a curved boundary, such as e.g., the well in this study, is expected to be lower when the problem is discretized on a Cartesian grid than when nodes are placed directly on the curved boundary using e.g., an unstructured grid. Before proceeding with the five simulations described in the previous section, it was therefore necessary to estimate how good was our representation of the circular well on a Cartesian grid. To this end, one simulation was run with a smooth-walled fracture of constant aperture and a Newtonian fluid, with the same geometry and boundary conditions as in the five simulations. The computed flow was perfectly radial as expected. The pressure distribution is shown in Fig. 2, and a comparison to the analytical solution is made in Fig. 3. The error with respect to the analytical solution is below 1.4 % everywhere in Fig. 3. This high precision is due to the high resolution in

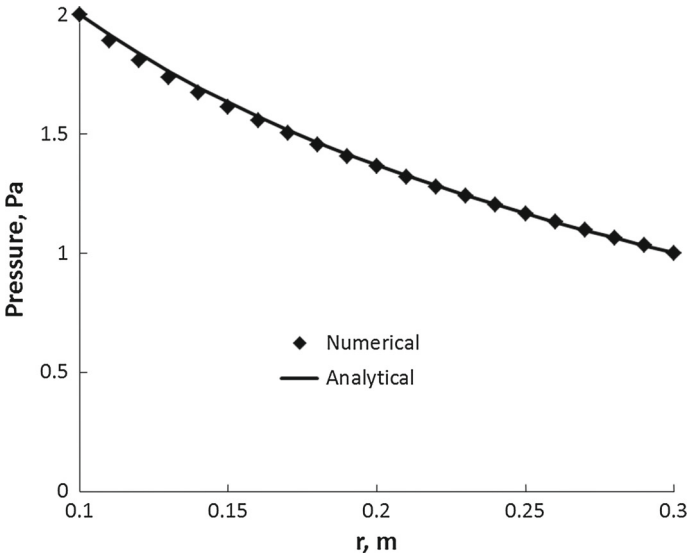

Fig. 3 Pressure distribution along $x = 0.32$ m in a smooth-walled fracture of constant aperture. r is the distance from the well center located at $x = y = 0.32$ m

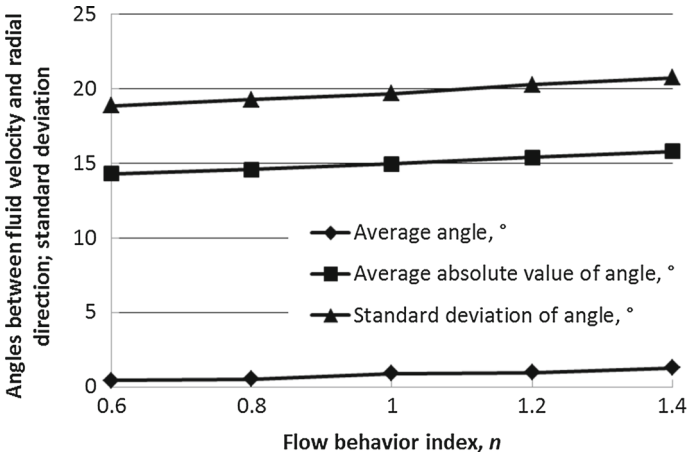

Fig. 4 The values of the average angle,$\langle\alpha\rangle$, average absolute value of angle, $\langle|\alpha|\rangle$ and standard deviation of angle, σ, between the fluid velocity and the radial direction, as functions of the flow behavior index

representing the well of 20 cm in diameter on a grid with 1 cm grid spacing. It was concluded that the model therefore provided a satisfactory representation of the circular well.

Simulations with the rough-walled fracture (Fig. 1) and different values of the flow behavior index, n, suggested that there was a systematic change in the steady-state flow pattern with varying n. In particular, the flow became slightly more radial with decreasing n. This is evident in Fig. 4, where the values of $\langle\alpha\rangle$, $\langle|\alpha|\rangle$ and σ introduced in Sect. 2 are plotted versus n. A comparison of visual appearances of the velocity field at different values of n suggests the same trend. As an example, the velocity fields obtained with three values of n, namely

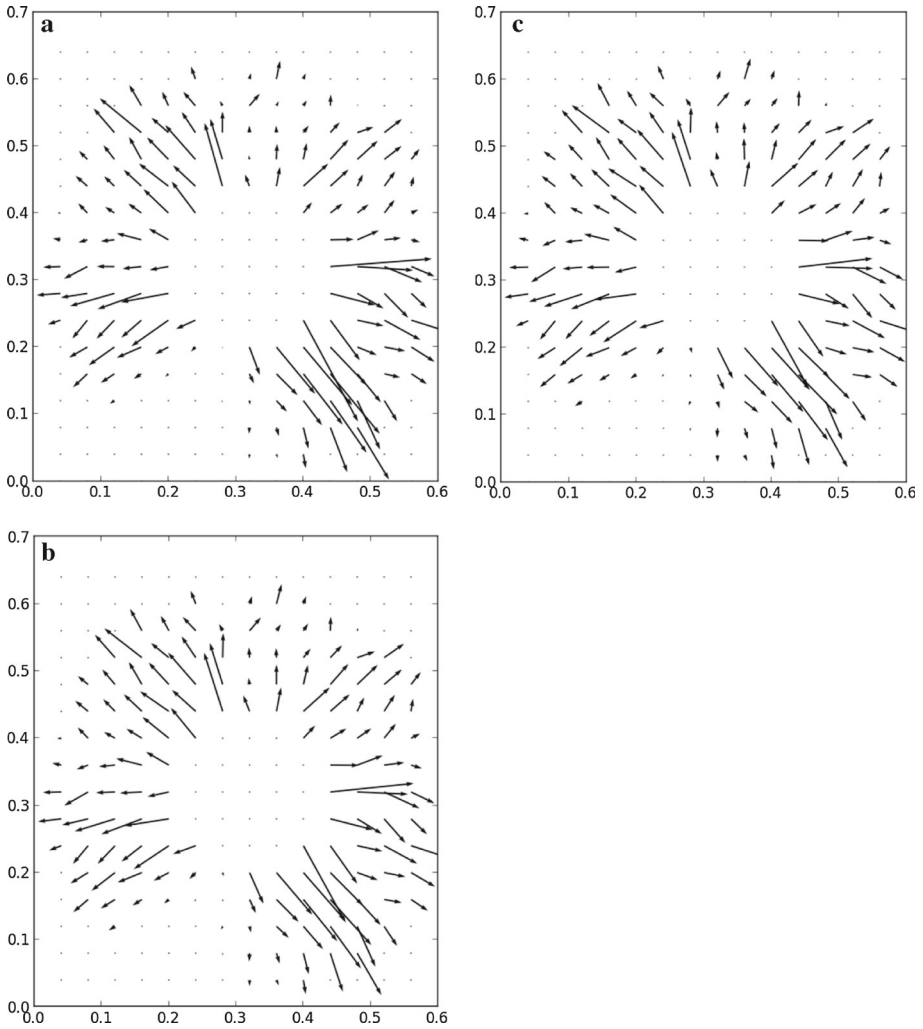

Fig. 5 Steady-state fluid velocity fields obtained with $n = 0.6$ (**a**), $n = 1.0$ (Newtonian, **b**) and $n = 1.4$ (**c**). Note the zero aperture region in the bottom left part of the fracture

$n = 0.6, n = 1.0$, and $n = 1.4$, are shown in Fig. 5a–c, respectively. Pressure distributions corresponding to Fig. 5a–c are shown in Fig. 6a–c, respectively.

The flow in Fig. 5 appears slightly more tortuous as n increases. This is in agreement with the result obtained earlier with a unidirectional flow where decreasing n led to the flow becoming more unidirectional (Lavrov 2013b).

The change in the flow pattern was further illustrated by the tracer front propagation. The front appeared more jagged at lower values of n (shear-thinning fluids). The front had a smoother appearance at higher values of n (shear-thickening fluids). As an example, concentration distributions before the tracer front reaches the outer boundary of the model are shown in Fig. 7a, b for $n = 0.6$ and $n = 1.4$, respectively.

The fracture in Fig. 1 has an area of zero aperture where the fracture faces come into contact with each other. This area appears in Fig. 5 as a zero-velocity region. During tracer

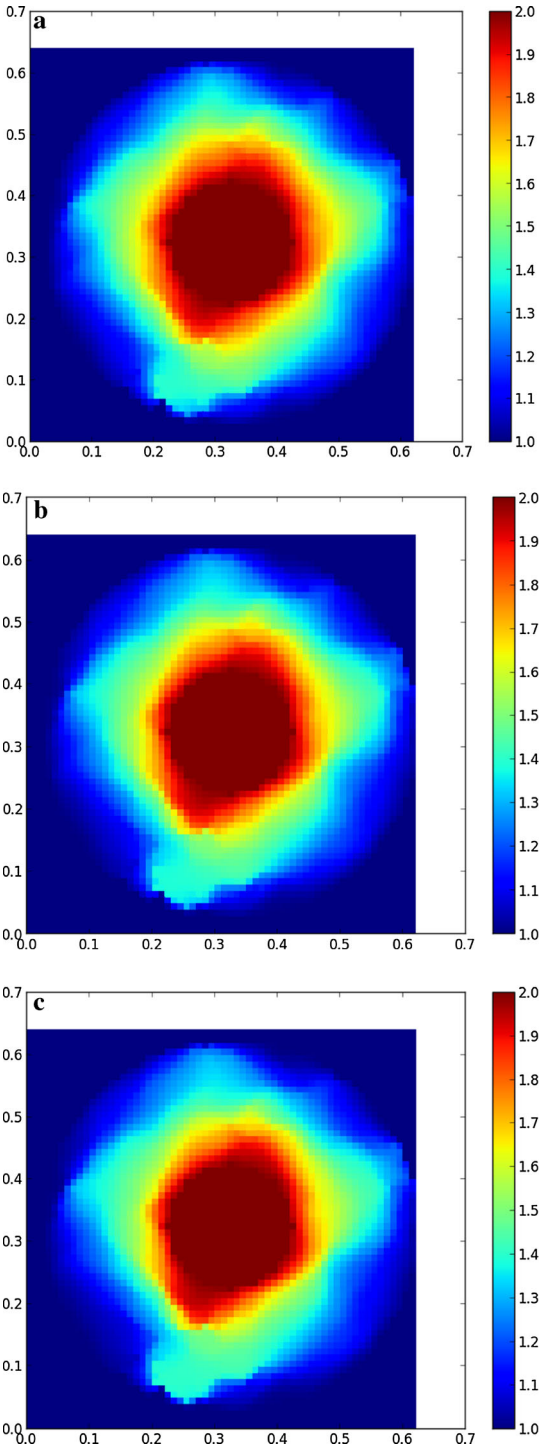

Fig. 6 Fluid pressure distributions in the fracture obtained with $n = 0.6$ (**a**), $n = 1.0$ (Newtonian, **b**) and $n = 1.4$ (**c**). Color bar in Pa. Horizontal and vertical dimensions of the plots in m

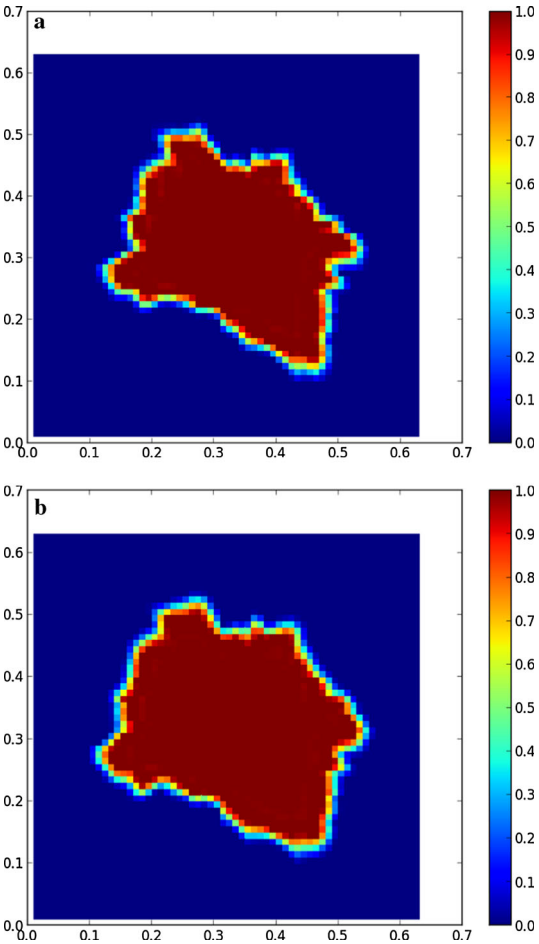

Fig. 7 Distributions of normalized tracer concentration at an early stage of injection: **a** $n = 0.6$; **b** $n = 1.4$. Concentration is normalized to the concentration in the injected fluid at well

injection, the fluid carries the tracer around this contact region. The difference in the velocity pattern at lower and higher n results in a different distribution of the tracer around the contact area at later stages of injection. As illustrated in Fig. 8b, in the case of $n = 1.4$, the fluid brings the tracer closer to the contact area which is enabled by the above-mentioned greater tortuosity of the flow as compared to the case of $n = 0.6$ (Fig. 8a).

The shape of the tracer propagation front in Fig. 7a, b is suggestive of a "dispersion" induced by asperities. This dispersion has nothing to do with molecular diffusion or Taylor dispersion which was not considered in the present study. The "dispersion" visible in Fig. 7 is purely due to the effect of asperities on the flow pattern.

The effect of n on the radial flow pattern and tracer transport in a rough-walled fracture can be understood by considering Eq. (2) or Table 1. The effective fluid viscosity, μ_{eff}, is given by

$$\mu_{\text{eff}} = \tau_{ij}/\dot{\gamma}_{ij} = C\dot{\gamma}^{n-1}. \tag{5}$$

Thus, for a shear-thinning fluid ($n < 1$), the effective viscosity is higher at lower shear rates than at higher shear rates. It is, therefore, higher in those parts of the fracture that have smaller aperture. For a shear-thickening fluid, on the contrary, the effective viscosity is smaller at

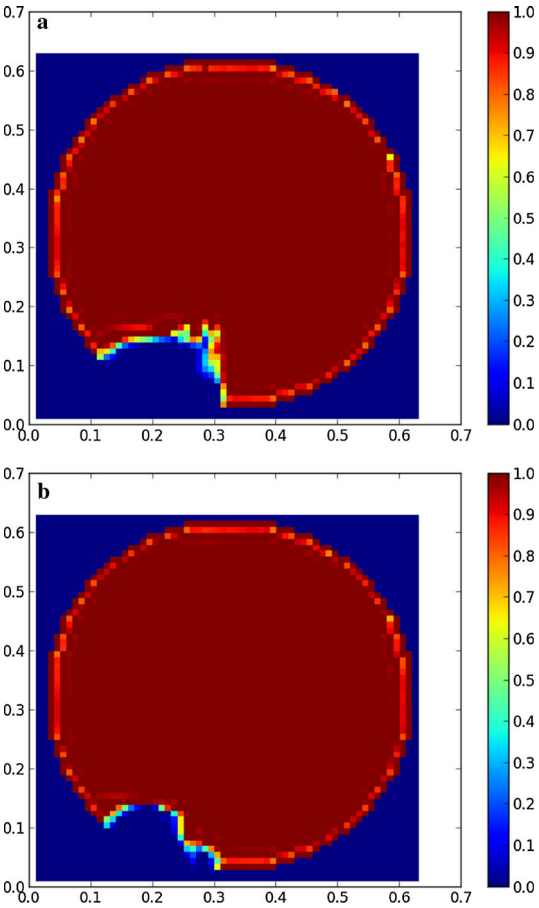

Fig. 8 Distributions of tracer concentration at a later stage of injection: **a** $n = 0.6$; **b** $n = 1.4$. Concentration is normalized to the concentration in the injected fluid at well

smaller shear rates than at higher shear rates. This makes it easier for a shear-thickening fluid to flow in the vicinity of contact areas between fracture faces, where the fracture aperture is relatively small. This is the reason why a shear-thickening fluid can come closer to closed contacts and, consequently, transport particles closer to the contacts. As a result, the flow of a shear-thinning fluid appears more directional (in the radial direction), while a shear-thickening fluid flows more easily around asperities, contributing to flow tortuosity. When a tracer is introduced, this flow pattern results in a more jagged tracer propagation front observed with a shear-thinning fluid.

It should be mentioned that one of the consequences of non-Newtonian rheology, apart from its effect on flow tortuosity, is the breakdown of the celebrated "cubic law." In the case of Newtonian fluid, the flow rate in a conduit with smooth parallel walls is known to be proportional to w^3 (e.g., Esaki et al. 1999). In the case of power-law rheology, Eq. (1) indicates that the flow rate is proportional to $w^{(2n+1)/n}$, which becomes the cubic law for $n = 1$. Thus, for shear-thinning fluids, the flow rate has an even stronger dependence on the aperture than for Newtonian fluids.

The results presented above have implications for particle transport and placement in fractures. Such particles can be e.g., proppant particles in hydraulic fracturing or particles of lost circulation materials in drilling, used to combat mud losses. Optimal placement of particles

in fractures is crucial to the success of those jobs: In well stimulation, proppant placement determines the eventual conductivity of the hydraulic fracture and thus the productivity of the well. In drilling, plugging a fracture with particles can be crucial for preventing or stopping the loss of an expensive drilling fluid and for reducing non-productive time on the rig (Majidi et al. 2010; Huang et al. 2011). The results presented above indicate that the placement of particles is affected by both, the fracture roughness and the fluid rheology. The assumption of a smooth-walled fracture, often used to design treatments in the industry, is therefore only valid as a first, crude approximation. The effect of fracture morphology should be part of routine tests of fluids with particulates, an approach that was recently employed by Guo et al. (2014).

As another direction of further work, the effect of fluid compressibility on the results presented herein might be worth looking at. This effect, though probably limited for non-Newtonian fluids (drilling or fracturing fluids), might be significant for flow of some Newtonian fluids in natural fractures, e.g., CO_2.

The simulation results presented in this paper require experimental verification and might provide an aid in designing future experiments. Moreover, since most drilling fluids are yield-stress fluids, an investigation of the effects of yield stress is needed. It might be expected that e.g., Bingham rheology will have even more pronounced effect on the flow pattern and particle distribution in a rough-walled fracture than a shear-thinning fluid without yield point.

4 Conclusions

Numerical simulations of radial flow of a non-Newtonian power-law fluid in a rough-walled fracture indicate that there is a slight, but systematic change in the flow pattern as the flow behavior index is varied. The flow becomes more radial when the flow behavior index is decreased, the fluid becoming more shear-thinning. The flow becomes more tortuous when the flow behavior index is increased, the fluid becoming more shear-thickening. The change in the flow pattern affects the tracer front propagation. The front appears more jagged with shear-thinning fluids. The front appears smoother with more shear-thickening fluids. A shear-thickening fluid is able to carry the tracer closer to a spot of zero aperture than a shear-thinning fluid is. The results of the study are relevant for fluid engineering in drilling and well stimulation applications where non-Newtonian fluids with particulates are injected into natural or man-induced fractures.

Acknowledgments The research presented herein was partially supported through the FP7-PEOPLE-2009-IAPP Marie Curie IAPP Project No. 251475. Three anonymous reviewers are gratefully acknowledged for their comments.

References

Aston, M.W., McLean, M.R.: A physical model for stress cages. SPE paper 90493 presented at the SPE annual technical conference and exhibition held in Houston, Texas, USA, 26–29 September 2004 (2004)

Auradou, H., Boschan, A., Chertcoff, R., Gabbanelli, S., Hulin, J.P., Ippolito, I.: Enhancement of velocity contrasts by shear-thinning solutions flowing in a rough fracture. J. Non-Newtonian Fluid Mech. **153**, 53–61 (2008)

Auradou, H., Boschan, A., Chertcoff, R., D'Angelo, M.-V., Hulin, J.-P., Ippolito, I.: Miscible transfer of solute in different model fractures: from random to multiscale wall roughness. C. R. Geosci. **342**, 644–652 (2010)

Balhoff, M., Sanchez-Rivera, D., Kwok, A., Mehmani, Y., Prodanović, M.: Numerical algorithms for network modeling of yield stress and other non-Newtonian fluids in porous media. Transp. Porous Media **93**, 363–379 (2012)

Brown, S.R.: Fluid flow through rock joints: the effect of surface roughness. J. Geophys. Res. B **92**, 1337–1347 (1987)

Cheon, D.S., Lee, H.K., Jeon, S., Lee, C.I.: A study of hydromechanical behaviours of rock joints using torsional shearing system. In: Siging, W., Bingjun, F., Zhongkui, L. (eds.) Frontiers of Rock Mechanics and Sustainable Development in the 21st Century, pp. 185–188 (2002)

Di Federico, V.: Estimates of equivalent aperture for non-Newtonian flow in a rough-walled fracture. Int. J. Rock Mech. Min. Sci. **34**, 1133–1137 (1997)

Esaki, T., Du, S., Mitani, Y., Ikusada, K., Jing, L.: Development of a shear-flow test apparatus and determination of coupled properties for a single rock joint. Int. J. Rock Mech. Min. Sci. **36**, 641–650 (1999)

Fournier, A., Fussell, D., Carpenter, L.: Computer rendering of stochastic models. Commun. ACM **25**, 371–384 (1982)

Glass, R.J., Rajaram, H., Nicholl, M.J., Detwiler, R.L.: The interaction of two fluid phases in fractured media. Curr. Opin. Colloid Interface Sci. **6**, 223–235 (2001)

Guo, Q., Cook, J., Way, P., Ji, L., Friedheim, J.E.: A comprehensive experimental study on wellbore strengthening. IADC/SPE paper 167957 presented at the 2014 IADC/SPE drilling conference and exhibition held in Fort Worth, Texas, USA, 4–6 March (2014)

Huang, J., Griffiths, D.V., Wong, S.-W.: Characterizing natural-fracture permeability from mud-loss data. SPE J. **16**(1), 111–114 (2011)

Koyama, T., Fardin, N., Jing, L.: Shear induced anisotropy and heterogeneity of fluid flow in single rock fracture by translational and rotatory shear displacements—a numerical study. Int. J. Rock Mech. Min. Sci. **41**(3), 426 (2004)

Koyama, T., Fardin, N., Jing, L., Stephansson, O.: Numerical simulation of shear-induced flow anisotropy and scale-dependent aperture and transmissivity evolution of rock fracture replicas. Int. J. Rock Mech. Min. Sci. & Geomech. Abstr. **43**, 89–106 (2006)

Koyama, T., Li, B., Jiang, Y., Jing, L.: Numerical modelling of fluid flow tests in a rock fracture with a special algorithm for contact areas. Comput. Geotech. **36**, 291–303 (2009)

Lavrov, A.: Stability and dispersion analysis of semi-Lagrangian method with Hermite interpolation. Numer. Heat Transfer, Part B: Fundam **55**, 177–195 (2009)

Lavrov, A.: Numerical modeling of steady-state flow of a non-Newtonian power-law fluid in a rough-walled fracture. Comput. Geotech. **50**, 101–109 (2013a)

Lavrov, A.: Redirection and channelization of power-law fluid flow in a rough-walled fracture. Chem. Eng. Sci. **99**, 81–88 (2013b)

Majidi, R., Miska, S.Z., Thompson, L.G., Zhang, J.: Quantitative analysis of mud losses in naturally fractured reservoirs: the effect of rheology. SPE Drilling & Completion, December, 509–517 (2010)

Mitani, Y., Esaki, T., Nakashima, Y.: An experimental study on the anisotropy of flow in a rock joint. 3rd Korea-Japan Joint Symp. on Rock Eng., Seoul, pp. 281–288 (2002)

Neuzil, C.E., Tracy, J.V.: Flow through fractures. Water Resour. Res. **17**, 191–199 (1981)

Nicholl, M.J., Glass, R.J.: Simulation of immiscible viscous displacement within the plane of a horizontal fracture. In: Elsworth, D., Tinucci, J.P., Heasley, K.A. (eds.) Rock Mechanics in the National Interest, pp. 205–210. Balkema, Amsterdam (2001)

Schmittbuhl, J., Steyer, A., Jouniaux, L., Toussaint, R.: Fracture morphology and viscous transport. Int. J. Rock Mech. Min. Sci. **45**, 422–430 (2008)

Staniforth, A., Côté, J.: Semi-Lagrangian integration schemes for atmospheric models—a review. Mon. Weather Rev. **119**, 2206–2223 (1991)

Vilarrasa, V.: Numerical modelling of fluid flow and particle transport in a riugh rock fracture during shear. M.Sc. Thesis, Technical University of Catalonia (2005)

Vilarrasa, V., Koyama, T., Neretnieks, I., Jing, L.: Shear-induced flow channels in a single rock fracture and their effect on solute transport. Transp. Porous Media **87**, 503–523 (2011)

Yang, Z., Niemi, A., Fagerland, F., Illangasekare, T.: Two-phase flow in rough-walled fractures: comparison of continuum and invasion–percolation models. Water Resour. Res. **49**, 993–1002 (2013)

Yeo, I.W., de Freitas, M.H., Zimmerman, R.W.: Effect of shear displacement on the aperture and permeability of a rock fracture. Int. J. Rock Mech. Min. Sci. **35**(8), 1051–1070 (1998)

Zimmerman, R.W., Kumar, S., Bodvarsson, G.S.: Lubrication theory analysis of the permeability of rough-walled fractures. Int. J. Rock Mech. Min. Sci. & Geomech. Abstr. **28**, 325–331 (1991)